J Nanopart Res (2014) 16:2143
DOI 10.1007/s11051-013-2143-y

RESEARCH PAPER

Photocatalytic activity of nitrogen-doped TiO_2-based nanowires: a photo-assisted Kelvin probe force microscopy study

Ming-Chung Wu · Hsueh-Chung Liao · Yu-Cheng Cho · Che-Pu Hsu · Ting-Han Lin · Wei-Fang Su · András Sápi · Ákos Kukovecz · Zoltán Kónya · Andrey Shchukarev · Anjana Sarkar · William Larsson · Jyri-Pekka Mikkola · Melinda Mohl · Géza Tóth · Heli Jantunen · Anna Valtanen · Mika Huuhtanen · Riitta L. Keiski · Krisztián Kordás

Received: 19 June 2013 / Accepted: 18 November 2013 / Published online: 4 December 2013

Abstract In this study, a set of nitrogen-doped TiO_2-based nanomaterials demonstrating photocatalytic activity was developed by combining the efforts of lattice doping and metal nanoparticle decoration and tested for photo-degradation of methylene blue dye by applying solar simulator irradiation. The surface potential shifts of these TiO_2-based photocatalytic nanomaterials measured by Kelvin probe force microscope have been used to study the degree of electron generation of the photocatalysts after irradiation and were well correlated with the photocatalytic activity. The nitrogen-doped TiO_2 nanowires decorated with Pt nanoparticles can induce obvious electron accumulation and result in a large shift of surface potential. The analysis shows a clear correlation between the surface potential shift and the photodegradation activity. Furthermore, a thorough comparative photocatalytic activity study combined with X-ray photoelectron spectroscopy analysis of the materials—doped with nitrogen under various conditions—reveals that the photocatalytic efficiency of the catalysts is maintained even if the lattice doping is leached e.g., by thermal treatments after doping.

Keywords Kelvin probe force microscopy · Photocatalyst · TiO_2 · Surface potential · Nanostructured catalyst · Photodegradation

Electronic supplementary material The online version of this article (doi:10.1007/s11051-013-2143-y) contains supplementary material, which is available to authorized users.

M.-C. Wu (✉) · T.-H. Lin
Department of Chemical and Materials Engineering, College of Engineering, Chang Gung University, Taoyuan 33302, Taiwan
e-mail: mingchungwu@mail.cgu.edu.tw

H.-C. Liao · Y.-C. Cho · C.-P. Hsu · W.-F. Su
Department of Materials Science and Engineering, National Taiwan University, Taipei 10617, Taiwan

A. Sápi · Á. Kukovecz · Z. Kónya
Department of Applied and Environmental Chemistry, University of Szeged, Rerrich Béla tér 1, Szeged 6720, Hungary

Á. Kukovecz
MTA-SZTE "Lendület" Porous Nanocomposites Research Group, Rerrich B. tér 1, Szeged 6720, Hungary

Z. Kónya
MTA-SZTE Reaction Kinetics and Surface Chemistry Research Group, Rerrich B. tér 1, Szeged 6720, Hungary

A. Shchukarev · A. Sarkar · W. Larsson · J.-P. Mikkola
Technical Chemistry, Department of Chemistry, Umeå University, 901 87 Umeå, Sweden

J.-P. Mikkola
Industrial Chemistry & Reaction Engineering, Process Chemistry Centre, Åbo Akademi University, 20500 Åbo-Turku, Finland

M. Mohl · G. Tóth · H. Jantunen · K. Kordás
Microelectronics and Materials Physics Laboratories, Department of Electrical Engineering, EMPART Research Group of Infotech Oulu, University of Oulu, P.O. Box 4500, 90014 Oulu, Finland

Introduction

Kelvin probe force microscopy (KPFM) technique adopts a non-contact tip with a conductive coating to measure the potential difference between the tip and the adjacent surface (Liscio et al. 2008; Glatzel et al. 2002; Hoppe et al. 2005; Palermo et al. 2007; Wu et al. 2010, 2013). The surface potential relates to and has an effect on a number of different surface phenomena, including those of catalytic activity, doping/impurities/defects, band-bending at interfaces, polarization of surfaces, etc. (Palermo et al. 2008; Chiesa et al. 2005; Glatzel et al. 2008). The assessed surface potential or work function map, with a resolution of a few nanometers produced by KPFM, gives useful information about the composition, surface charge distribution, and electronic states on the surface of a solid (Wu et al. 2009; Liu and Li 2010; Zhang et al. 2013). A great number of recent studies have utilized KPFM to obtain the simultaneous mapping of both structural and electronic properties of conjugated polymer-based photovoltaic materials. KPFM has been reported to be capable of obtaining quantitative mappings in a non-contact and non-destructive manner, rendering it attractive for the analysis of for instance organic materials (Palermo et al. 2006). The technique was also to be found useful upon measuring the work function of thin heterostructures, thus enabling its engineering for catalytic applications (Bieletzki et al. 2010). Furthermore, correlation between shifts in the surface potential (surface potential difference in the presence or absence of illumination) and the power conversion efficiency of polymer photovoltaic devices based on poly(3-hexylthiophene) (P3HT) and titanium dioxide nanorod (TiO_2 NR) hybrid bulk heterojunctions could also be assessed by KPFM (Wu et al. 2010). When applied in ultrahigh vacuum, a tenfold improvement of the spatial resolution may be achieved (Spadafora et al. 2010). Just recently, our group demonstrated that KPFM can also be used to predict the photocatalytic activity of materials which could open up new avenues in the field of photocatalysis (Wu et al. 2013).

A. Valtanen · M. Huuhtanen · R. L. Keiski
Mass and Heat Transfer Process Laboratory, Department of Process and Environmental Engineering, University of Oulu, P.O. Box 4300, 90014 Oulu, Finland

For some 40 years, TiO_2 and its enormous number of derivatives have been in the mainstream of studies related to photocatalysis (Sarkar et al. 2012). The reasons are straightforward; the availability, affordability, good photocatalytic activity/stability of TiO_2, and its suitability for practical applications, e.g., in air and waste water purification, defogging and self-cleaning surfaces, hydrogen generation as well as an ingredient in hybrid polymers as well as dye-sensitized solar cells (Khan et al. 2002; Lee et al. 2012; Liao et al. 2012; Saif et al. 2012; Wu et al. 2011a, b). The recent discoveries of large-scale hydrothermal synthesis of various types of titanate nanotubes and nanowires opened further possibilities for titania-related nanomaterials research, viz. the 1-dimensional titanates may be converted to self-similar TiO_2-based nanowires (Horvath et al. 2007; Bamwenda et al. 1995; Wu et al. 2011a, 2012). The titanate-to-titania conversion process is robust as it only requires process steps easily scalable and industrially applicable such as ion-exchange, calcination, doping, and surface decoration (Buso et al. 2007; Feist and Davies 1992; Lin et al. 2008; Qi et al. 2011; Wu et al. 2011a, 2012).

Nitrogen doping of TiO_2 can somewhat decrease the band gap due to the introduced new states in the forbidden band (Asahi et al. 2001; Spadavecchia et al. 2012). Moreover, when TiO_2 (being an n-type semiconductor) is brought in contact with other semiconducting (p-type) or metallic (large work function) nanoparticles, rectifying junctions evolve at the interface, which can contribute to an improved charge separation of the photo-generated electron–hole pairs by disabling undesired electron–hole recombination (Linsebigler et al. 1995; Wu et al. 2011a). Hence, efforts that combine lattice doping and metal nanoparticle decoration with the recent achievements of titanate/titania nanofiber synthesis attracted a lot of interest in order to develop novel and efficient photocatalyst materials (Wu et al. 2011a, 2012, 2013).

In the present study, a set of nitrogen-doped TiO_2-based photocatalysts was studied. Titanate nanotubes and nanowires were synthesized by the hydrothermal method and subjected to a consequent annealing with ammonia or air and ammonia, to obtain N-doped TiO_2 nanowires (N–TiO_2 NWs). Optical absorption and the first-principle calculations were carried out to address

the photocatalytic mechanism of TiO_2 with and without nitrogen doping. Afterward, the N–TiO_2 NWs were decorated with Pt nanoparticles by a wet impregnation process. Photo-assisted KPFM was used to detect the charge response on the surface of the as-prepared photocatalysts, in the presence and absence of visible and UV-B light irradiation. Consequently, we found that the surface potential shifts of photocatalysts were closely correlated to their photocatalytic activity. On the other hand, we also investigated the role of N-doping in terms of the change of photocatalytic activity of TiO_2 nanoparticles and nanowires. A comprehensive set of experimental data on the correlation between Ti and N bond concentration assessed by X-ray photoelectron spectroscopy (XPS) and photocatalytic H_2 generation from ethanol:water mixtures was evaluated.

Experimental

Preparation of TiO_2-based nanowires

Sodium hydrogen titanate nanotubes (SHT NTs) were synthesized by the alkali hydrothermal process. In a typical synthesis, 50.0 g of TiO_2 powder (Anatase E 171, Kemira) was dispersed in a volume of 1.00 L of 10.0 M aqueous NaOH (Molar Chemical Ltd.) by continuous stirring for 2 h. The suspension was then treated in a revolving autoclave (with a volume of 1400 mL) at 130 °C for 24 h. The obtained solid fraction of the dispersion was then rinsed with deionized water and 0.10 M HCl solution until the solution became nearly neutral and chloride ion free. N–TiO_2 nanowires (N–TiO_2 NWs) were synthesized by the calcination of SHT NTs at 600 °C for 15 h in 2 % NH_3 (in N_2 buffer). Anchoring of Pt or Pd nanoparticles onto the surface of N–TiO_2 NWs was carried out by means of wet impregnation. In a typical process, 4.10 mg platinum (II) acetylacetonate (Aldrich, 99.99 %) or 5.80 mg palladium (II) acetylacetonate (Aldrich, 99 %) was dissolved in 40.0 mL acetone and mixed with 200.00 mg of N–TiO_2 by ultrasonic agitation for 3 h and conventional stirring for 6 h. After evaporating the solvents at $\sim$50 °C under N_2 atmosphere, the samples were annealed in air at 300 °C for 2 h to decompose the metal complexes, and then reduced in 15 % H_2 (in Ar) flow at 500 °C for 4 h. Finally, N–TiO_2–Pd nanowires and N–TiO_2–Pt nanowires with $\sim$1.0 wt% nominal metal load were obtained.

To study the effect of nitrogen leaching on the photocatalytic performance of the N-doped photocatalyst samples, nanowires of TiO_2 and their derivatives were synthesized from titanate nanowires. The main difference in the preparation was the temperature of hydrothermal synthesis (175 °C instead of 130 °C), otherwise the doping and decoration steps were following similar procedures as described above for the nanowires made from titanate nanotubes.

Characterization of TiO_2 nanowires

The photocatalytic activity of SHT NTs, N–TiO_2 NWs, N–TiO_2–Pd NWs, N–TiO_2–Pt NWs, and the reference—commercial TiO_2 nanoparticles ($\sim$25 nm, Aldrich) were tested in the degradation of methylene blue, which is a commonly used model reaction in photocatalysis. In a typical experiment, 20.0 mg of catalyst was sonicated for 2 min in 50 ml methylene blue (Acros) aqueous solution having concentration of 10 mg/L. The suspension was irradiated with solar simulator (Newport 92193, 100 mW/cm^2) under vigorous stirring, at ambient conditions. Before the actual photodegradation experiments, the suspensions were left to relax for 10 min in order to minimize the error of the dye concentration measurements caused by initial surface adsorption. After centrifuging for 15 min at 5000 rpm, the absorption spectrum of the retained methylene blue and its derivatives in the supernatant was recorded (Absorption Spectrophotometer, Lambda 35, Perkin-Elmer) in the 300–900 nm wavelength range. The concentrations of the methylene blue were calculated from the absorbance at $\lambda = 662$ nm extrapolated to a previously plotted calibration curve. The microstructures of the photocatalysts were studied by transmission electron microscopy (EFTEM, LEO 912 OMEGA, 120 kV) as well as by X-ray diffraction (XRD, Siemens D5000 and Philips PW 1380, both using Cu Kα radiation).

Photo-Kelvin probe force microscopy measurement

Surface potential mapping was measured by a Kelvin probe force microscopy (Digital Instruments, Nanoscope III), at room temperature. Conductive tips were used to obtain the surface potential data. A cantilever

of n-type silicon (Nanosensors) with an average force constant of ~2.8 N/m (resonance frequency of ~75 kHz) was coated with chromium and a Pt–Ir5 alloy. The TiO_2-based catalysts were dispersed in ethanol solution and dropped on a gold surface of 100 nm thickness (coated on a silicon wafer). After drying, a line scan in tapping mode AFM was applied to acquire topographic data and then, along the same line, another scan was performed but with the tip lifted to a distance of 20 nm from the surface while a voltage V_{DC} was applied at the tip to compensate for the electrostatic oscillations. The as-measured surface potential map of the TiO_2 catalysts was assessed in dark and also under the illumination of either a halogen lamp (Royal Philips Electronics, 139, 50 W) or a UV-B lamp (Sankyo Denki, G8T5E, 8 W). From here on, the differences in the surface potential measured in dark versus light conditions ($SP_{dark} - SP_{light}$) are referred as the surface potential shift (*SP* shift).

Computational simulation

DFT computational simulation analysis was performed with Perdew–Burke–Ernzerhof functional implemented in generalized gradient approximation (GGA) and in CASTEP (Cambridge Serial Total Energy Package) that applies plane waves to expand the electron wave function. In the calculations for band gap, the density of states (DOS), and absorption spectrum, a (2 × 3 × 1) supercell with nitrogen and platinum impurities is considered (norm-conserving pseudopotential, energy cut-off of 450.0 eV, and k-point set of 1 × 1× 2).

Results and discussion

Structure and composition of the photocatalyst synthesized from titanate nanotubes

Sodium hydrogen titanate nanotubes (SHT NTs) were synthesized by means of an alkali-mediated hydrothermal process. The length of SHT NTs obtained was up to several hundreds of nanometers with an inner diameter of ~5 nm and outer diameter of ~10 nm (Fig. 1a). After calcination at 600 °C for 12 h under ammonia flow, N–TiO_2 NWs (nanowires) with rough surface were obtained (Fig. 1b). Despite the acid treatment applied before the calcination, the product N–TiO_2 NWs still contained ~12.3 at.% of sodium as measured by XPS. TEM images of N–TiO_2 NWs decorated with Pd nanoparticles (N–TiO_2–Pd NWs) and Pt nanoparticles (N–TiO_2–Pt NWs) are shown in Fig. 1c, d respectively. Based on the TEM analysis, the Pd- and Pt-nanoparticles are distributed homogeneously all over the surface of TiO_2 nanofibers and show uniform size distributions with an average particle diameters of 3.5 nm ± 1.4 and 2.5 nm ± 0.5 nm, respectively.

Fig. 1 TEM images of **a** sodium hydrogen titanate nanotubes, **b** nitrogen-doped anatase TiO_2 nanowires, **c** Pd-decorated N–TiO_2 nanowires, and **d** Pt-decorated N–TiO_2 nanowires. *Insets* in **c** and **d** show the corresponding Pd and Pt metal nanoparticle size distributions

According to our previous studies (Wu et al. 2011a, 2012), calcination at 600 °C results in the formation of anatase phase only. The intensity of reflections increases with temperature, indicating better ordering of the lattice. However, at temperatures above 600 °C, formation of the catalytically less active rutile phase is initiated, as shown by the appearance of its (110) reflection at ~27.2° of 2θ [PDF #77-0445]. XRD patterns of N–TiO_2 NWs confirm that the SHT NTs calcined at 600 °C for 15 h under ammonia atmosphere are transformed to anatase TiO_2 phase as shown in Fig. 2. Reflections can be perfectly indexed as the body-centered tetragonal lattice structure [PDF #89-4921] of anatase TiO_2, with lattice constants of $a = b = 3.78$ and $c = 9.50$ Å, respectively. For N–TiO_2–Pd NWs and N–TiO_2–Pt NWs, the XRD patterns show no difference compared to the parent N–TiO_2.

According to XPS analysis summarized in Table 1 and in Fig. 3, respectively, N–TiO_2 NWs show a new component in the N 1s peak at 395.9 eV that can be assigned to the formation of Ti–N bond, i.e., substitutional N in the lattice (Wang et al. 2009). The other components with higher binding energies around ~398.4 and ~400.1 eV correspond to interstitial N and the decomposed products of NH_3 molecules, respectively. The Pd $3d_{5/2}$ component at 336.7 eV shows the presence of Pd^{2+} (17 % of the total Pd amount), due to partially oxidized metal particles emerging on the surface of N–TiO_2–Pd NWs. Both Pt and Pd have lower binding energies of metallic state than that reported in XPS database (Pt $4f_{7/2}$: 71.2 eV, Pd $3d_{5/2}$: 335.1 eV) which can be assigned to the size effect or the increased electron density on the metal

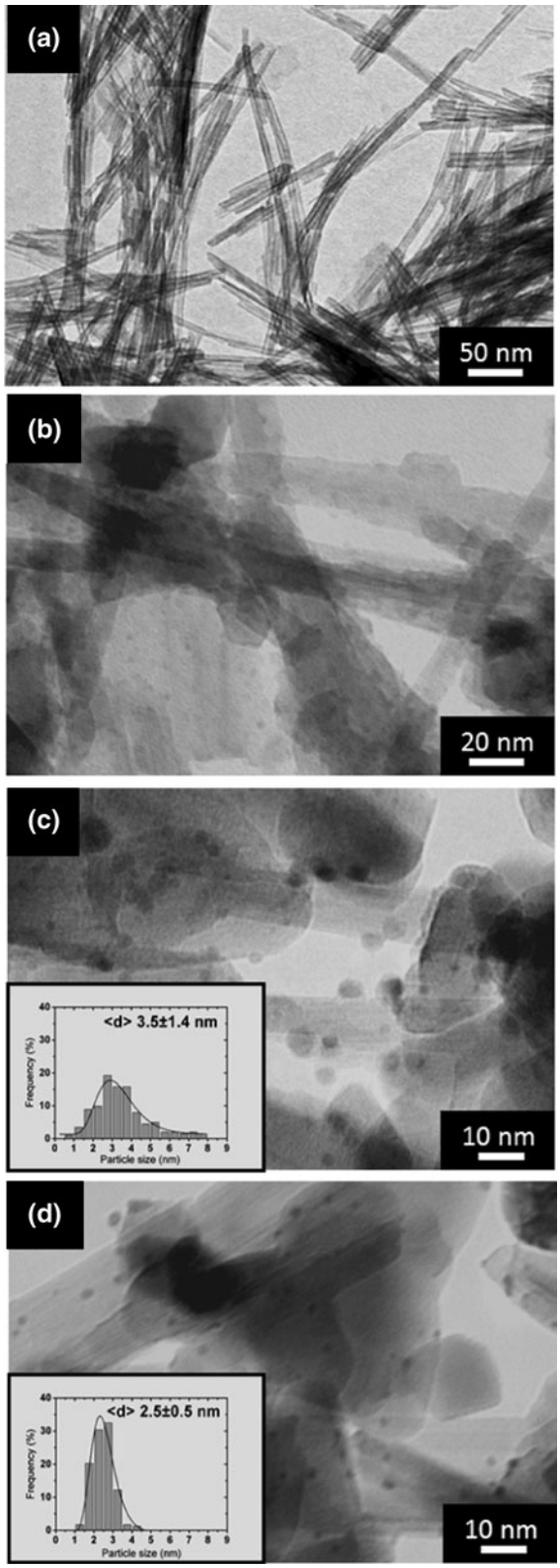

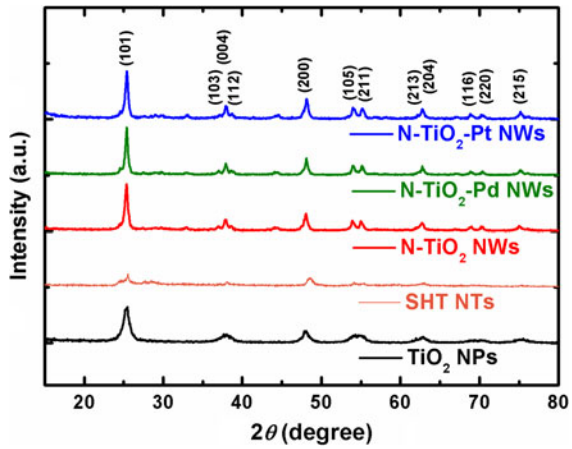

Fig. 2 XRD patterns of commercial TiO_2 nanoparticles (TiO_2 NPs), sodium hydrogen titanate nanotubes (SHT NTs), nitrogen-doped anatase TiO_2 nanowires (N–TiO_2 nanowires), Pd-decorated N–TiO_2 nanowires (N–TiO_2–Pd NWs), and Pt-decorated N–TiO_2 nanowires (N–TiO_2–Pt NWs)

surfaces from nanoparticles (active site)–support interaction (Roy et al. 2007).

The normalized absorption spectra of TiO_2 NPs, SHT NTs, N–TiO_2 NWs, N–TiO_2–Pd NWs, and N–TiO_2–Pt NWs are shown in Fig. 4. The comparison result of the absorption spectra of these photocatalysts shows the evidence of higher absorptivity in the visible region for the photocatalysts with nitrogen doping and/or metal nanoparticles decoration.

The projected DOS (calculated by GGA-PBE functional implemented in CASTEP) for pristine TiO_2 and N–TiO_2 (Fig. 5) demonstrates that the doped nitrogen mainly contributes to the states near valence band edge ($\sim$0 eV) and narrows the band gap (Wang et al. 2009).

The photocatalytic activity of the commercial TiO_2 nanopaticles (TiO_2 NPs), sodium hydrogen titanate nanotubes (SHT NTs), N–TiO_2 nanowires (N–TiO_2 NWs), N–TiO_2–Pd nanowires (N–TiO_2–Pd NWs), and N–TiO_2–Pt nanowires (N–TiO_2–Pt NWs) were evaluated in a solar simulator utilizing the light-induced photodegradation of methylene blue in aqueous solution. The UV–Vis spectra of methylene blue as a function of visible light irradiation time were recorded, and from the absorbance measured at $\lambda = 662$ nm, the methylene blue concentration was calculated using a calibration curve measured previously. TiO_2-catalyzed photodegradation of different dyes essentially follows the first-order Langmuir–Hinshelwood kinetics as $\ln(c_0/c) = kt$, where c and c_0

Table 1 XPS peak position and the corresponding atomic ratio of N–TiO_2 nanowires, N–TiO_2–Pd nanowires, and N–TiO_2–Pt nanowires

Sample	N 1s peak position and the corresponding N/Ti atomic ratio (%)	Ti $2p_{3/2}$ peak position	Pd $3d_{5/2}$ peak position and the corresponding Pd/Ti atomic ratio (%)	Pt $4f_{7/2}$ peak position and the corresponding Pt/Ti atomic ratio (%)
N–TiO_2 NWs	0.74 % at 395.9 eV 0.61 % at 398.4 eV 1.43 % at 400.1 eV	458.5 eV	Not detected	Not detected
N–TiO_2–Pd NWs	0.27 % at 395.8 eV 0.50 % at 398.4 eV 1.54 % at 400.0 eV	458.5 eV	1.48 % at 334.6 eV 0.72 % at 335.4 eV 0.46 % at 336.6 eV	Not detected
N–TiO_2–Pt NWs	0.34 % at 396.0 eV 0.59 % at 398.3 eV 1.18 % at 399.9 eV	458.5 eV	Not detected	0.95 % at 70.6 eV 0.23 % at 71.5 eV

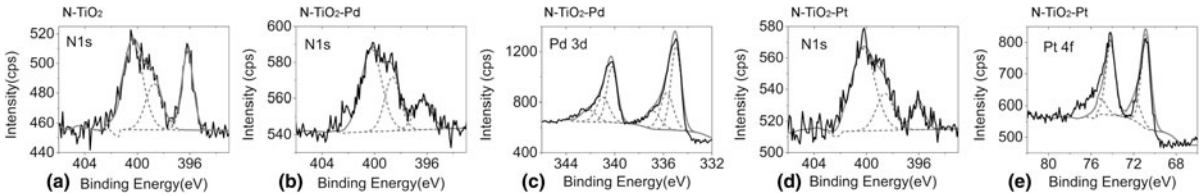

Fig. 3 **a** X-ray photoelectron spectra of N 1s component for TiO_2 nanowires that are (**a**) N-doped, (**b**) N-doped and then Pd-decorated, and (**d**) N-doped and then Pt-decorated. **c** and **e** show the corresponding core level spectra for Pd and Pt, respectively. *Note* The N-doped TiO_2 nanowires were obtained by annealing titanate nanotubes in ammonia

are the concentration of the dye at time t *and* $t = 0$, and k is the reaction rate constant (Katti et al. 2009; Wu et al. 2011a). As expected, our experimental data also obey this kinetics (Fig. 6). The rate constant of the reaction on SHT NTs shows the smallest value of $\sim 0.0036\ \text{min}^{-1}$. For the sake of comparison, the corresponding rate constant obtained for the reference material, commercial TiO_2 NPs, is in the range of $\sim 0.0259\ \text{min}^{-1}$. An addition of Pd- and Pt-cocatalyst particles significantly increased the observed value of the rate constant, i.e., from $0.0099\ \text{min}^{-1}$ of N–TiO_2 NWs to 0.0456 and $0.0499\ \text{min}^{-1}$ of N–TiO_2–Pd NWs and N–TiO_2–Pt, respectively.

In this study, KPFM was also used to obtain the surface potential mapping of each photocatalyst in the presence and absence of illumination, including either visible or UV-B light similar to that studied earlier on TiO_2 nanowires synthesized from titania nanowires (Wu et al. 2013). Each photocatalyst was drop-cast on a silicon substrate coated with a thin film of gold. The responses of the surface potential under visible light were weak, while significant variations of the surface

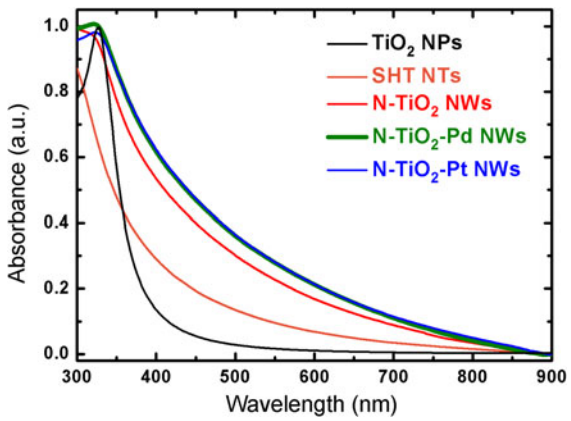

Fig. 4 Absorption spectra of sodium hydrogen titanate nanotubes (SHT NTs), nitrogen-doped anatase TiO_2 nanowires (N–TiO_2 nanowires), Pd-decorated N–TiO_2 nanowires (N–TiO_2–Pd NWs), and Pt-decorated N–TiO_2 nanowires (N–TiO_2–Pt NWs), respectively

potential under UV light were observed. The obtained surface potential mappings without (Fig. 7a-1, b-1, c-1) and with (Fig. 7a-2, b-2 and c-2) 1-h UV-B

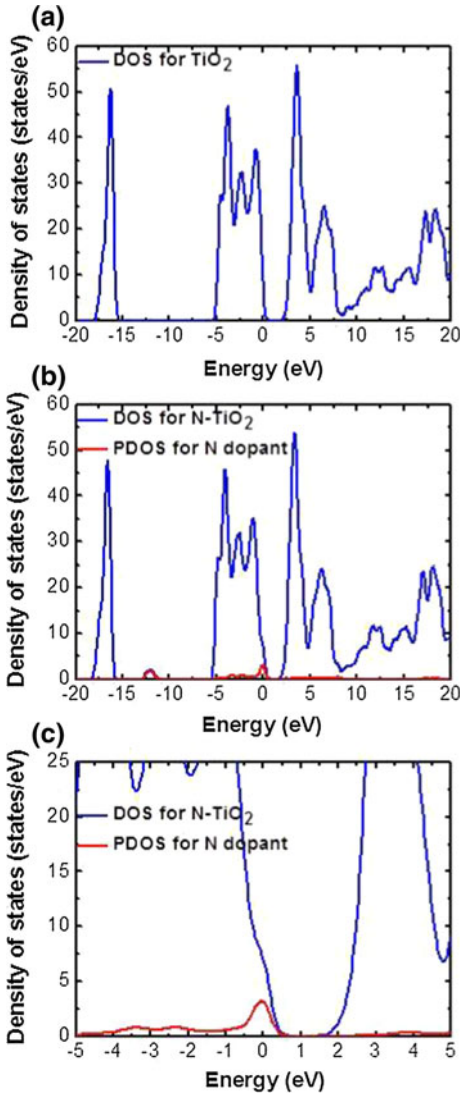

Fig. 5 Density of states for **a** TiO_2, **b** N–TiO_2, and **c** enlarged section near the Fermi level of (**b**)

illumination are shown in Fig. 7. The insets of the surface potential mappings show the corresponding topographic images. The values of the surface potential across the white dotted line can be easily compared in case of the presence and absence of illumination as shown in Fig. 7a-3, b-3, c-3 and Fig. 7a-4, b-4, c-4, respectively. SHT NTs exhibit almost no change (smaller than 5 mV) while in the case of the N–TiO_2 NWs and N–TiO_2–Pt NWs, considerable negative shifts of −10 and −40 mV, respectively, were observed. Note that the detected response reaches the stable surface potential after continuous illumination for 1 h. Consequently, this

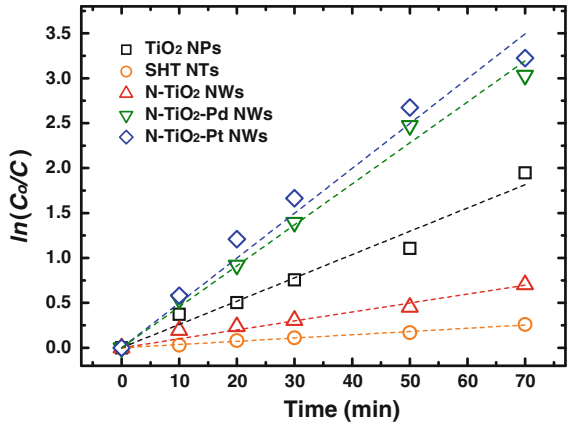

Fig. 6 Kinetic plots for the photodegradation of methylene blue using different types of photocatalysts under the solar simulator illumination

observation can be attributed to the inefficient carrier transport in the bulk TiO_2 aggregation. In other words, a single nanotube is about 10 nm in diameter, while the TiO_2 for KPFM investigation is nearly 200 nm in thickness; indicating that several tens of TiO_2 nanotubes are bundled together. Upon illumination, the excited free carriers are difficult to transport to the ground (Au substrate) across the boundaries between the nanotubes or nanowires. Therefore, the excited carriers gradually accumulate on the surfaces which can be detected by the KPFM tip. The negative shift for N–TiO_2 material (Fig. 7b), is assumed to cause by band gap reduction induced by nitrogen doping; which may result in better light absorption efficiency and, consequently, to a larger potential shift in the KPFM measurements. Moreover, the obvious negative shift for N–TiO_2–Pt NWs under UV excitation, compared to N–TiO_2 NWs, seems to correlate with greater efficiency in the photodecoloration reaction of methylene blue. The considerable negative shift of the surface potential indicates an efficient accumulation of electrons on the surface due to light excitation. Noble metals, such as Pt, Pd, and Au, decorated on TiO_2-based materials have been found to enhance the activity of the photocatalyst due to the rectifying Schottky barrier formed at the interface between the metal nanoparticles and the TiO_2 photocatalysts. Therefore, N–TiO_2–Pt NWs shows not only larger negative shift of surface potential, but also better photocatalytic activity. This relation could serve as an excellent guideline when the photocatalytic activity is determined using KPFM methodology.

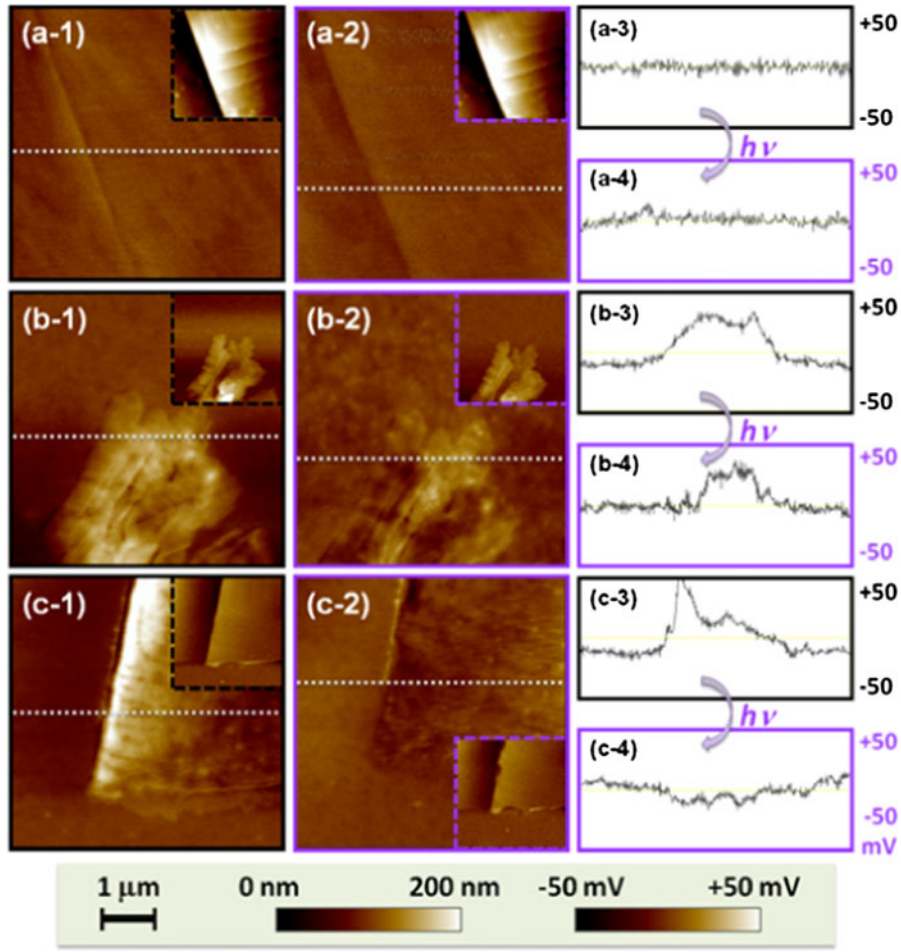

Fig. 7 Surface potential mappings in the *dark* (**a-1**, **b-1**, **c-1**) and under UV-B illumination (**a-2**, **b-2**, **c-2**) of three kinds of nanomaterials, (**a**) SHT NTs, (**b**) N–TiO_2 NWs, and (**c**) N–TiO_2–Pt NWs, on gold thin film. The *insets* of surface potential mappings are topographic images. (**a-3**, **b-3**, **c-3**) and (**a-4**, **b-4**, and **c-4**) are surface potential values of the cross section obtained from the corresponding *white-dotted line* without and under UV-B illumination, respectively. Image size is 5 × 5 µm

The effect of N-leaching on the catalytic performance

Decoration of N-doped nanowires with metals (more accurately the subsequent high-temperature annealing) can result in a considerable decrease of the concentration of N–Ti bonds in the structure (Table 1). In order to find out whether this phenomenon has any influence on the photocatalytic performance of the materials, we study a number of different N-doped TiO_2 materials (including nanowires and nanoparticles) with and without the decorating metals. According to XPS analysis, the degree of N-leaching depends very much on the synthesis conditions and structure of the starting materials. When the N-doped TiO_2 nanowires are obtained from titania nanotubes in a single-step annealing in NH_3, the subsequent metal decoration step (that includes annealing in air and in H_2 gas) causes a drop of the Ti–N bond concentration (component at ~396.0 eV) (Table 1). In the case where the nanowires are synthesized from titanate nanowires (not nanotubes) by a direct annealing in NH_3, we observed a similar decrease of the N:Ti ratio for the Ti–N bond (see supplementary information Table S1) after metal decoration. On the other hand, when N-doping was performed by annealing titania (not titanate) nanowires or nanoparticles in NH_3, the substitutional nitrogen, i.e., the Ti–N bonds seems to disappear after metal decoration as peaks near 396 eV could not be resolved with our XPS instrument (see supplementary information Tables S1, S2; Fig. 8a, b.

Despite the decreased concentration, or even elimination of Ti–N bonds, the catalyst materials still remain very active according to the performed model reaction (photocatalytic hydrogen generation from ethanol) shown in Fig. 8c. To elucidate the role of nitrogen

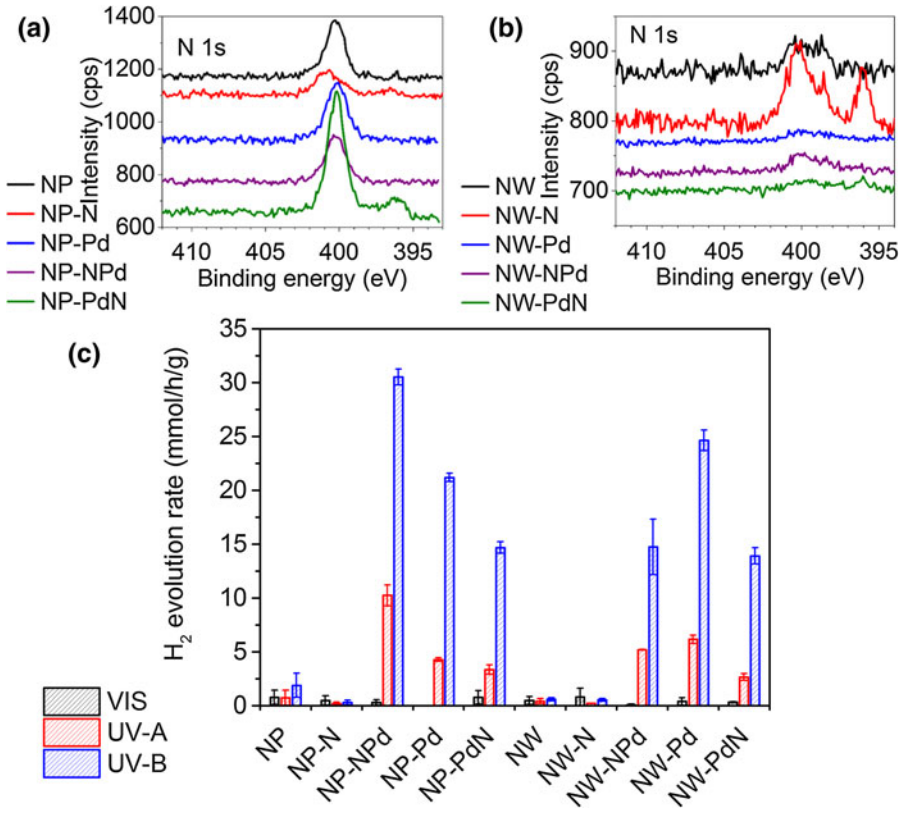

Fig. 8 X-ray photoelectron spectra of N 1s component for **a** nanoparticles and **b** nanowires of TiO_2 and their N-doped and Pd-decorated derivatives. **c** Shows the photocatalytic H_2 production rates of the corresponding nanomaterials from 50 vol% ethanol (in water) using visible, UV-A, and UV-B irradiation

doping, we compared 5–5 sets of catalyst nanoparticles and nanowires. In each set, pristine TiO_2 nanoparticles (NP) and nanowires (NW); their N-doped derivatives (NP–N and NW–N); their Pd-decorated derivatives (NP–Pd and NW–Pd); their N-doped and then Pd-decorated derivatives (NP–N–Pd and NW–N–Pd) as well as Pd-decorated and then N-doped derivatives (NP–Pd–N and NW–Pd–N) were studied. From the X-ray photoelectron spectra of the N 1s component it is clear that the sequence of metal decoration and nitrogen doping makes a significant difference for the composition of the material obtained: The samples that are doped first with nitrogen and then decorated with metal (i.e., NP–N–Pd and NW–N–Pd) loose the doping (missing peak of Ti–N at $\sim$396 eV), while the ones N-doped after metal decoration (i.e., NP–N–Pd and NW–N–Pd) are truly doped. Interestingly, the samples that lost their substitutional nitrogen (i.e., NP–NPd and NW–N–Pd) are still very active, even more than those that were doped after metal decoration.

The observed phenomenon is unexpected and the explanation for it is not entirely clear. We assume that the preserved hydrogen production capability in the case of N-doped and subsequently metal-decorated TiO_2 nanoparticles and nanowires can be attributed to the oxygen defects that are left behind after the cleavage of substituent nitrogen atoms from the lattice. An STM investigation showed that N-doped anatase subjected to an annealing step contains increased amounts of disordered oxygen-deficient areas and surface reconstructions (Batzill et al. 2006). On the one hand, the enhanced catalytic efficiency observed can alternatively be explained by the substantial raise in the number of oxygen vacancy defects that function as active sites during the reaction (Fujino et al. 2001). On the other hand, black-colored TiO_2, with lattice disorders introduced by hydrogen doping, has been shown to exhibit significant increase in the photocatalytic hydrogen production that can be assigned to mid-gap electronic states, accompanied by a reduced band gap (Chen et al. 2011). We believe that the reduction process applied during metal decoration may have induced further lattice disorders in the TiO_2 nanostructures, which are also manifested in a color change (graying) and elevated H_2 production efficiency.

Conclusions

The surface potential shifts of the photocatalysts measured by photo-kelvin probe force microscope have been used to study the degree of electron generation of the photocatalysts after irradiation and can be well correlated with the photocatalytic performance based on methylene blue decoloration. Noble metals decorated on the TiO_2-based catalysts were found to induce electron accumulation and result in larger shifts of the surface potential. Consequently, there is a clear correlation between the surface potential shift and their photocatalytic activity. The results of this study can serve not only as a useful guide for discovering new effective photocatalysts for the applications of photodegradation of dyes but also as a convenient analysis method for improving the photocatalytic performance of the materials prepared.

Although the positive effects of N-doping on the photocatalytic activity and on the increased surface potential shift are known and also supported by the data we reported here, we must note that the photocatalytic activity is not a direct function of the amount of substitutional nitrogen. As we have shown in this work, the samples seem to retain their activity even after high-temperature annealing and partial or complete loss of the substitutional N dopant, which indicate that defects may also play a significant role in the overall activity of TiO_2-based photocatalyst materials.

Acknowledgments The authors are grateful for financial support received from National Science Council of Taiwan (102-2633-E-182-001 and 102-2622-E-182-005-CC3), Chang Gung University Research Project, Finnish Funding Agency for Technology and Innovation (project, Imphona), Academy of Finland (project, Optifu), European Union Framework Programme 7 (project, Napep) as well as Kempe Foundations and Bio4Eneregy program in Sweden. The financial support of TÁMOP-4.2.2.A-11/1/KONV-2012-0047 project is acknowledged.

References

Asahi R, Morikawa T, Ohwaki T, Aoki K, Taga Y (2001) Visible-light photocatalysis in nitrogen-doped titanium oxides. Science 293:269. doi:10.1126/science.1061051

Bamwenda GR, Tsubota S, Nalamura T, Haruta M (1995) Photoassisted hydrogen production from a water-ethanol solution: a comparison of activities of Au–TiO_2 and Pt–TiO_2. J Photochem Photobiol A 89:177. doi:10.1016/1010-6030(95)04039-I

Batzill M, Morales EH, Diebold U (2006) Influence of nitrogen doping on the defect formation and surface properties of TiO_2 rutile and anatase. Phys Rev Lett 96:026103. doi:10.1103/PhysRevLett.96.026103

Bieletzki M, Hynninen T, Soini TM, Pivetta M, Henry CR, Foster AS, Esch F, Barth C, Heiz U (2010) Topography and work function measurements of thin MgO(001) films on Ag(001) by nc-AFM and KPFM. Phys Chem Chem Phys 12:3203. doi:10.1039/b923296f

Buso D, Pacifico J, Martucci A, Mulvaney P (2007) Gold-nanoparticle-doped TiO_2 semiconductor thin films: optical characterization. Adv Funct Mater 17:347. doi:10.1002/adfm.200600349

Chen X, Liu L, Yu PY, Mao SS (2011) Increasing solar absorption for photocatalysis with black hydrogenated titanium dioxide nanocrystals. Science 331:746. doi:10.1126/science.1200448

Chiesa M, Bürgi L, Kim JS, Shikler R, Friend RH, Sirringhaus H (2005) Correlation between surface photovoltage and blend morphology in polyfluorene-based photodiodes. Nano Lett 5:559. doi:10.1021/nl047929s

Feist TP, Davies PK (1992) The soft chemical synthesis of TiO_2(B) from layered titanates. J Solid State Chem 101:275. doi:10.1016/0022-4596(92)90184-W

Fujino T, Katayama M, Inudzuka K, Okuno T, Oura K, Hirao T (2001) Surface hydroxyl formation on vacuum-annealed TiO_2(110). Appl Phys Lett 79:2716. doi:10.1063/1.1412427

Glatzel T, Fuertes Marrón D, Schedel-Niedrig T, Sadewasser S, Lux-Steiner MC (2002) $CuGaSe_2$ solar cell cross section studied by Kelvin probe force microscopy in ultrahigh vacuum. Appl Phys Lett 81:2017. doi:10.1063/1.1506205

Glatzel T, Rusu M, Sadewasser S, Lux-Steiner MC (2008) Surface photovoltage analysis of thin CdS layers on polycrystalline chalcopyrite absorber layers by Kelvin probe force microscopy. Nanotechnology 19:145705. doi:10.1088/0957-4484/19/14/145705

Hoppe H, Glatzel T, Niggemann M, Hinsch A, Lux-Steiner MC, Sariciftci NS (2005) Kelvin probe force microscopy study on conjugated polymer/fullerene bulk heterojunction organic solar cells. Nano Lett 5:269. doi:10.1021/nl048176c

Horvath E, Kukovecz A, Konya Z, Kiricsi I (2007) Hydrothermal conversion of self-assembled titanate nanotubes into nanowires in a revolving autoclave. Chem Mater 19:927. doi:10.1021/cm062413q

Katti A, Venna SR, Carreon MA (2009) Self-assembly hydrothermal assisted synthesis of mesoporous anatase in the presence of ethylene glycol. Catal Commun 10:2036. doi:10.1016/j.catcom.2009.07.026

Khan S, Al-Shahry M, Ingler WB Jr (2002) Efficient photochemical water splitting by a chemically modified n-TiO_2. Science 297:2243. doi:10.1126/science.1075035

Lee KM, Wu SJ, Chen CY, Wu CG, Ikegami M, Miyoshi K, Miyasaka T, Ho KC (2012) Efficient and stable plastic dye-sensitized solar cells based on a high light-harvesting ruthenium sensitizer. J Mater Chem 19:5009. doi:10.1039/b903852c

Liao WP, Hsu SC, Lin WH, Wu JJ (2012) Hierarchical TiO_2 nanostructured array/P3HT hybrid solar cells with

interfacial modification. J Phys Chem C 116:15938. doi:10.1039/b903852c

Lin CH, Chao JH, Liu CH, Chang JC, Wang FC (2008) Effect of calcination temperature on the structure of a Pt/TiO_2(B) nanofiber and its photocatalytic activity in generating H_2. Langmuir 24:9907. doi:10.1021/la800572g

Linsebigler AL, Lu G, Yates JT Jr (1995) Photocatalysis on TiO_n Surfaces: Principles, Mechanisms, and Selected Results. Chem Rev 95:735. doi:10.1021/cr00035a013

Liscio A, Luca GD, Nolde F, Palermo V, Müllen K, Samorì P (2008) Photovoltaic charge generation visualized at the nanoscale: a proof of principle. J Am Chem Soc 130:780. doi:10.1021/ja075291r

Liu L, Li G (2010) Electrical characterization of single-walled carbon nanotubes in organic solar cells by Kelvin probe force microscopy. Appl Phys Lett 96:083302. doi:10.1063/1.3332489

Palermo V, Palma M, Samorì P (2006) Electronic characterization of organic thin films by Kelvin probe force microscopy. Adv Mater 18:145. doi:10.1002/adma.200501394

Palermo V, Ridolfi G, Talarico AM, Favaretto L, Barbarella G, Camaioni N, Samorì P (2007) A Kelvin probe force microscopy study of the photogeneration of surface charges in all-thiophene photovoltaic blends. Adv Funct Mater 17:472. doi:10.1002/adfm.200600122

Palermo V, Otten MBJ, Liscio A, Schwartz E, de Witte PAJ, Castriciano MA, Wienk MM, Nolde F, De Luca G, Cornelissen JJLM, Janssen RAJ, Müllen K, Rowan AE, Nolte RJM, Samorì P (2008) The relationship between nanoscale architecture and function in photovoltaic multichromophoric arrays as visualized by Kelvin probe force microscopy. J Am Chem Soc 130:14605. doi:10.1021/ja804069n

Qi F, Moiseev A, Deubener J, Weber A (2011) Thermostable photocatalytically active TiO_2 anatase nanoparticles. J Nanopart Res 13:1325. doi:10.1007/s11051-010-0211-0

Roy S, Hegde MS, Ravishankar N, Madras G (2007) Creation of redox adsorption sites by Pd^{2+} ion substitution in nanoTiO_2 for high photocatalytic activity of CO oxidation, NO reduction, and NO decomposition. J Phys Chem C 111:8153. doi:10.1021/jp066145v

Saif M, Aboul-Fotouh SMK, El-Molla SA, Ibrahim MM, Ismail LFM (2012) Improvement of the structural, morphology, and optical properties of TiO_2 for solar treatment of industrial wastewater. J Nanopart Res 14:1227. doi:10.1007/s11051-012-1227-4

Sarkar A, Shchukarev A, Leino A-R, Kordas K, Mikkola J-P, Petrov PO, Tuchina ES, Popov AP, Darvin ME, Meinke MC, Lademann J, Tuchin VV (2012) Photocatalytic activity of TiO_2 nanoparticles: effect of thermal annealing under various gaseous atmospheres. Nanotechnology 23:475711. doi:10.1088/0957-4484/23/47/475711

Spadafora EJ, Demadrille R, Ratier B, Grvin B (2010) Imaging the carrier photogeneration in nanoscale phase segregated organic heterojunctions by kelvin probe force microscopy. Nano Lett 10:3337. doi:10.1021/nl101001d

Spadavecchia F, Ardizzone S, Cappelletti G, Oliva C, Cappelli S (2012) Time effects on the stability of the induced defects in TiO_2 nanoparticles doped by different nitrogen sources. J Nanopart Res 14:1301. doi:10.1007/s11051-012-1301-y

Wang J, Tafen DN, Lewis JP, Hong ZL, Manivannan A, Zhi MJ, Li M, Wu NQ (2009) Origin of photocatalytic activity of nitrogen-doped TiO_2 nanobelts. J Am Chem Soc 131:12290. doi:10.1021/ja903781h

Wu MC, Lin YY, Chen S, Liao HC, Wu YJ, Chen CW, Chen YF, Su WF (2009) Enhancing light absorption and carrier transport of P3HT by doping multi-wall carbon nanotubes. Chem Phys Lett 468:64. doi:10.1016/j.cplett.2008.11.080

Wu MC, Wu YJ, Yen WC, Lo HH, Lin CF, Su WF (2010) Correlation between nanoscale surface potential and power conversion efficiency of P3HT/TiO_2 nanorod bulk heterojunction photovoltaic devices. Nanoscale 2:1448. doi:10.1039/B9NR00385A

Wu MC, Hiltunen JT, Sápi A, Avila A, Larsson W, Liao HC, Huuhtanen M, Tóth G, Shchukarev A, Laufer N, Kukovecz A, Konya Z, Mikkola JP, Keiski R, Su WF, Chen YF, Jantunen H, Ajayan PM, Vajtai R, Kordás K (2011a) Nitrogen-doped anatase nanofibers decorated with noble metal nanoparticles for photocatalytic production of hydrogen. ACS Nano 5:5025. doi:10.1021/nn201111j

Wu MC, Sápi A, Avila A, Szab M, Hiltunen J, Huuhtanen M, Tóth G, Kukovecz A, Konya Z, Keiski R, Su WF, Jantunen H, Kordás K (2011b) Enhanced photocatalytic activity of TiO_2 nanofibers and their flexible composite films: decomposition of organic dyes and efficient H_2 generation from ethanol–water mixtures. Nano Res 4:360. doi:10.1007/s12274-010-0090-9

Wu MC, Tóth G, Sápi A, Leino AR, Konya Z, Kukovecz A, Su WF, Kordás K (2012) Synthesis and photocatalytic performance of titanium dioxide nanofibers and the fabrication of flexible composite films from nanofibers. J Nanosci Nanotechnol 12:1421. doi:10.1166/jnn.2012.4655

Wu MC, Liao HC, Cho YC, Tóth G, Chen YF, Su WF, Kordás K (2013) Photo-Kelvin probe force microscopy for photocatalytic performance characterization of single filament of TiO_2 nanofiber photocatalysts. J Mater Chem A 1:5715. doi:10.1039/c3ta01011b

Zhang Q, Deng X, Qian PZG, Wang X (2013) Spatial modelling for refining and predicting surface potential mapping with enhanced resolution. Nanoscale 5:921. doi:10.1039/C2NR33603K